# Fluorine-donating electrolytes enable highly reversible 5-V-class Li metal batteries

Liumin Suo[a,b,c], Weijiang Xue[b,c], Mallory Gobet[d], Steve G. Greenbaum[d], Chao Wang[b,c], Yuming Chen[b,c], Wanlu Yang[e], Yangxing Li[e,1], and Ju Li[b,c,1]

[a]Key Laboratory for Renewable Energy, Beijing Key Laboratory for New Energy Materials and Devices, Beijing National Laboratory for Condensed Matter Physics, Institute of Physics, Chinese Academy of Sciences, 100190 Beijing, China; [b]Department of Nuclear Science and Engineering, Massachusetts Institute of Technology, Cambridge, MA 02139; [c]Department of Materials Science and Engineering, Massachusetts Institute of Technology, Cambridge, MA 02139; [d]Department of Physics and Astronomy, Hunter College of City University of New York, New York, NY 10065; and [e]Watt Laboratory, Central Research Institute, Huawei Technologies Co., Ltd., 518129 Shenzhen, China

Edited by Thomas E. Mallouk, The Pennsylvania State University, University Park, PA, and approved December 18, 2017 (received for review July 24, 2017)

**Lithium metal has gravimetric capacity ∼10× that of graphite which incentivizes rechargeable Li metal batteries (RLMB) development. A key factor that limits practical use of RLMB is morphological instability of Li metal anode upon electrodeposition, reflected by the uncontrolled area growth of solid–electrolyte interphase that traps cyclable Li, quantified by the Coulombic inefficiency (CI). Here we show that CI decreases approximately exponentially with increasing donatable fluorine concentration of the electrolyte. By using up to 7 m of Li bis(fluorosulfonyl)imide in fluoroethylene carbonate, where both the solvent and the salt donate F, we can significantly suppress anode porosity and improve the Coulombic efficiency to 99.64%. The electrolyte demonstrates excellent compatibility with 5-V $LiNi_{0.5}Mn_{1.5}O_4$ cathode and Al current collector beyond 5 V. As a result, an RLMB full cell with only 1.4× excess lithium as the anode was demonstrated to cycle above 130 times, at industrially significant loading of 1.83 mAh/cm$^2$ and 0.36 C. This is attributed to the formation of a protective LiF nanolayer, which has a wide bandgap, high surface energy, and small Burgers vector, making it ductile at room temperature and less likely to rupture in electrodeposition.**

electrolyte | Li metal battery | $LiNi_{0.5}Mn_{1.5}O_4$ | Li metal anode | high voltage

Nonrechargeable batteries like Li/$SOCl_2$ can achieve 650 Wh/kg and 1,280 Wh/L at full-cell level, demonstrating the enormous advantage of Li metal anode (LMA). However, to make rechargeable batteries that can charge hundreds of times, the Coulombic efficiency (CE) and growth of porosity of LMA must get under control. In terms of anode gravimetric and volumetric capacity, while fully dense Li metal enjoys a huge advantage at the beginning (gravimetric capacity: 3,861 mAh/g; volumetric capacity: 3,861 mAh/g × 0.534 g/cm$^3$ = 2,062 mAh/cm$^3$, where 0.534 g/cm$^3$ is the theoretical density of Li metal), it would quickly form a large amount of dead lithium and gain porosity (1) upon redeposition in typical organic electrolytes. When the non–Li-metal volume fraction ϕ grows beyond 70%, the LMA volumetric capacity would drop below that of graphite (372 mAh/g × 1.6 g/cm$^3$ = 600 mAh/cm$^3$), at which point it is no longer commercially viable. The gain in porosity and interfacial area of LMA can be attributed to an effectively negative interfacial energy $\gamma_{LMA} < 0$, since thermodynamically all liquid electrolytes are unstable at 0 V vs. Li/Li$^+$, and will reductively decompose to form solid–electrolyte interphase (SEI) that covers every electron-conductive surface of LMA, incentivizing growth of the interfacial area. This explosive areal growth will cause electrolyte dry-out, as well as exhaustion of cyclable lithium (2, 3). The latter is semiquantitatively reflected by the CE and Coulombic inefficiency (CI ≡ 1 − CE), which characterizes the ratio of Li$^+$ that can be pulled out of the anode within a fixed cell voltage window, after a known amount of Li$^+$ is deposited into it in the same voltage window, assuming only Li$^+$ can be transferred in the electrolyte in a nonblocking manner (4) and the anode is initially free of cyclable lithium. There is an industry lore that in order for a Li-matched full cell to cycle 200 times, CE needs to exceed 99.9% (CI < $10^{-3}$). Even though this is not exact (4), there is no question that an excellent CE is key for highly reversible LMA.

The most effective way to enhance the full-cell energy density is to introduce high-voltage and -capacity electrodes. Take the electrochemical couple of 5-V-class spinel $LiNi_{0.5}Mn_{1.5}O_4$ (LNMO)/LMA for example: This combination is likely to bring totally about 80% increase in full-cell energy density compared with commercial lithium-ion battery (LIB) with 4-V-class cathodes and graphite anode. However, 5-V rechargeable lithium metal battery (RLMB) is currently limited by the unavailability of electrolytes which must simultaneously satisfy wide enough electrochemical stability window, good compatibility with LNMO electrode, Al current collector corrosion resistance, and superior reversibility of LMA. Traditionally, carbonate-based electrolytes were exclusively used in commercial LIB thanks to its wide electrochemical stability window (0∼4.5 V) and robust SEI on the graphite anode, enabling the high voltage of LIB (5). But, they cannot work well in RLMB due to low CE for LMA [propylene carbonate (PC): CE < 80%, ethylene carbonate (EC): <95%, dimethyl carbonate (DMC): <30%, EC-DMC: <91%, and EC-diethyl carbonate (DEC): <95%] (6–11). Highly concentrated electrolytes have attracted much attention recently (12–24). On the cathode side, highly concentrated fluorine-organic Li salt electrolyte has been used to prevent the corrosion of Al current collector (18, 19, 25), as well as improving oxidative stability of cathode (17, 20, 22). With highly concentrated Li bis(fluorosulfonyl)imide (LiFSI) in DMC (1:1.1 by molar ratio), Li ion full cell (LiNMO/graphite) present very good cycling stability

## Significance

**Rechargeable lithium metal battery (RLMB) is the holy grail of high-energy-density batteries. If lithium metal anode (LMA) could be combined with 5-V $LiNi_{0.5}Mn_{1.5}O_4$ cathode, energy density could exceed 600 Wh/kg based on the cathode and anode electrode mass. Despite such promises, 5-V RLMB is still a vacant research space so far due to the unavailability of electrolytes which simultaneously satisfy a wide enough electrochemical stability window, good compatibility with $LiNi_{0.5}Mn_{1.5}O_4$, and superior reversibility of LMA. In this work, a class of full-fluoride (FF) electrolyte is invented for 5-V RLMB which not only has good compatibility with cathode and a wide stability window but also possesses the capability to make LMA more stable and reversible.**

Author contributions: L.S. and J.L. designed research; L.S. performed research; L.S., W.X., M.G., and S.G.G. contributed new reagents/analytic tools; L.S., C.W., Y.C., W.Y., Y.L., and J.L. analyzed data; and L.S. and J.L. wrote the paper.

The authors declare no conflict of interest.

This article is a PNAS Direct Submission.



[1]To whom correspondence may be addressed. Email: liju@mit.edu or li.yangxing@huawei.com.

This article contains supporting information online at www.pnas.org/lookup/suppl/doi:10.1073/pnas.1712895115/-/DCSupplemental.

(17). On the LMA side, ether-based highly concentrated electrolytes [LiFSI-dimethyl ether (DME) (21), LiTFSI-DME-1,3-dioxolane (DOL) (23), and $LiCF_3SO_3$-tetraethylene glycol dimethyl ether (TEGDME) (26)] manifest high Li reversibility and good compatibility with sulfur and oxygen cathodes (21, 23). However, because ethers decompose violently at cathode potential higher than 4 V vs. $Li/Li^+$, its application is strictly restricted in RLMBs whose operating voltage is below 4 V, thereby limiting the full-cell energy density (*SI Appendix*, Tables S1–S4).

The positive effect of fluorine donation on LMA is empirically known, through ex situ surface treatment by fluorine-containing gases ($CF_4$ and $C_2F_6$), and in-situ LiF-rich SEI formation by introducing F-containing additives such as HF (27), LiF (28, 29), fluoroethylene carbonate (FEC) (30), and $LiPF_6$ (31). Li is one of the most electropositive elements on the periodic table, while F is the most electronegative, and also has the smallest ionic radius among all anions. Therefore, LiF possesses many extreme properties among solids, such as the largest bandgap (13.6 eV) and the widest electrochemical stability window (32). This makes LiF an excellent SEI passivation component since a very thin LiF nanolayer can stop electron tunneling. Ozhabes et al. (33) showed by ab initio calculations that LiF has very high surface energy $\gamma$ and low Li adatom surface diffusion barrier; they attributed the large $\gamma >$ 0 not only to the electronegativity difference, but also to the small lattice constant (LiCl, the second smallest lithium halide, has a surface area 1.6× that of LiF). Therefore, adding nanoscale LiF to the SEI should increase the formation energy of the SEI, thereby reducing the magnitude of the negative $\gamma_{LMA}$ which promotes interfacial area growth. Finally, from a mechanical stability viewpoint, according to the Griffith fracture criterion, a ceramic with large surface energy is more resistant to fracture. Indeed, LiF is known to be able to deform plastically by dislocation glide due to its small Burgers vector (34, 35), rare among ceramics at room temperature. This mechanical and electrochemical stability compared with, say, $Li_2CO_3$ or $Li_2O$ could be essential in explaining the relative morphological stability of LMA with LiF protection during Li redeposition and volume expansion, as we will discuss below. For all these reasons, we believe the degree of fluorine donation, which controls LiF formation, is a key parameter in predicting good electrolytes for RLMB. Meanwhile, because of the extreme bandgap and electrochemical stability, LiF is also effective in protecting the cathode. In the work below, we correlate the donatable fluorine concentration (DFC) of many liquid electrolytes with CI of the LMA, and show that CI decays nearly exponentially with increasing DFC. Guided by this rule, a class of high-concentration full-fluoride (HFF) electrolytes with a large DFC is designed for 5-V RLMBs. Our preferred organic solvents are carbonic esters due to their thermodynamic stability and good compatibility with LNMO. To drive up DFC, a fluorinated cyclic carbonic ester (FEC) was used as the sole solvent. Previously, FEC was only used as an additive (<10 wt %) (36, 37). FEC is expected to have dual purposes of stabilizing LMA imparted by LiF-rich SEI formation and enhancing oxidation stability of electrolyte (25). At the same time, a fluorine-organic Li salt (LiFSI) is utilized, considering its high yield of LiF upon decomposition (38).

The systematic role of donatable fluorine on the reversibility of LMA is evaluated by the average ⟨CE⟩ via "clean-slate" Li deposition–stripping on Cu foil (Fig. 1). To identify the trend, the logarithm of the average Li-cycling ⟨CI⟩ ($\log_{10}$ (100⟨CI⟩)) is shown in the vertical axis (39), with the corresponding cycling details shown in *SI Appendix*, Figs. S1 and S2. Obviously ⟨CI⟩ is highly dependent on DFC. Taking 1 m concentration electrolyte, for example, ⟨CI⟩ is above 50% in fluoride-free electrolyte (1 m $LiClO_4$ in PC), but falls dramatically to 31.6% and even less than 20% when $LiClO_4$ is replaced by fluorine-organic salts, LiTFSI and LiFSI, respectively. Impressively, in the case of full-fluoride–based (FF) system constituted by 1 m LiFSI in fluorinated carbonate

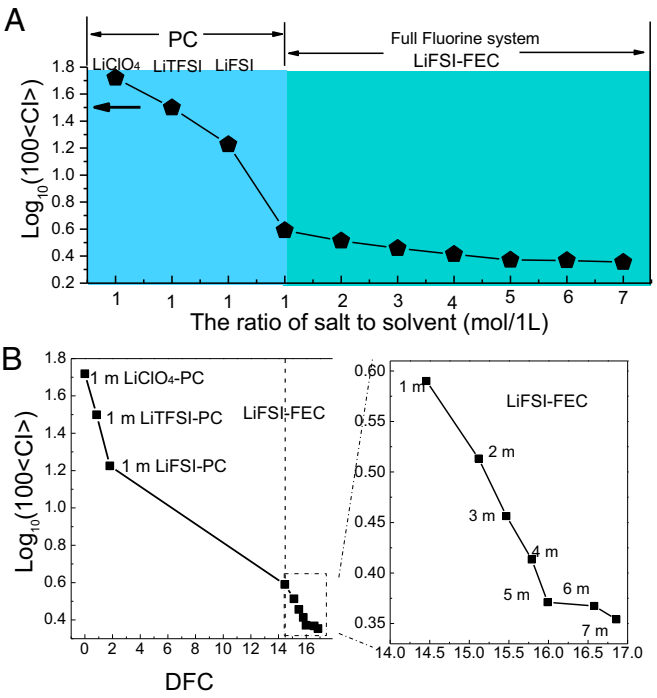


**Fig. 1.** Effect of a liquid electrolyte's DFC on the reversibility of LMA. CE is calculated from the galvanostatic deposition–stripping on Cu foil. One first pulls out all of the $Li^+$ one can pull out in a copper-backed anode, making sure there is no cyclable Li reserve (although SEI, which contains noncyclable Li, can exist physically) on the anode. One then electrochemically deposits $Q_{re}$ fresh $Li^+$ to the anode with $U_{max} \rightarrow U_{min}$, in the form of metallic lithium with varying degree of porosity. Lastly, one pulls $Q_{ox}$ $Li^+$ out of the anode with $U_{min} \rightarrow U_{max}$, and computes CE $\equiv Q_{ox}/Q_{re}$. ($I$ = 0.5 mA, $Q_{re}$ = 0.5 mAh). (*A*) Average ⟨CI⟩ of 1 m $LiClO_4$, 1 m LiTFSI, 1 m LiFSI in PC (averaged over the first 50 cycles), and the FF-based LiFSI-FEC binary system in the range of 1 m~7 m (averaged over the first 100 cycles), respectively. (*B*) Monotonic decreasing and roughly exponential relationship between ⟨CI⟩ and DFC.

(FEC), LMA exhibits extreme high reversibility with a very low ⟨CI⟩ < 4% when averaged over 100 cycles. ⟨CI⟩ also depends on the salt concentration in FF. With increasing ratio of LiFSI to FEC, ⟨CI⟩ monotonously drops (Fig. 1*A*) from 4% in 1 m FF to 2.3% in HFF (7 m). Based on the data above, it is clear that ⟨CI⟩ has a strong negative correlation with donatable fluorine of the liquid electrolyte. Note that donatable fluorine is not the absolute F amount in the electrolyte but the active F atomic content in salt/solvent whose reduction effectively generates LiF in SEI. As shown by molecular simulations of Li salt and solvent reductions (40, 41), the number of LiF generated per $LiClO_4$, LiTFSI, LiFSI, and FEC molecule is 0, 1, 2, and 1, respectively. DFC is thus defined straightforwardly as the molar sum of donatable F of salt and solvent molecules in 1 L electrolyte solution (detailed calculations can be found in *SI Appendix*, Table S5). As shown in Fig. 1*B*, ⟨CI⟩ decays nearly exponentially with DFC across many electrolytes.

LMA exhibits excellent cycling stability in HFF electrolyte. As shown in Fig. 2*A*, the voltage polarization of Li deposition–dissolution at 0.25 $mA/cm^2$ is very symmetrical with nearly no increase in 200 cycles (polarization: 60 mV at the 100th and 200th cycles) and, subsequently, with a slight increase to 70 mV at the 300th cycle and 90 mV at the 400th cycle. As the cycle number increases, ⟨CE⟩ continuously increases from 97.7% at the first 100 cycles to 99.64% during the 300th~400th cycles, indicating a self-healing mechanism (Fig. 2*B*) (39). The typical charge–discharge polarizations at different rates (0.25, 0.50, and 1.00 $mA/cm^2$) are 60, 140, and 160 mV, respectively, with ⟨CE⟩ of 98.37% and

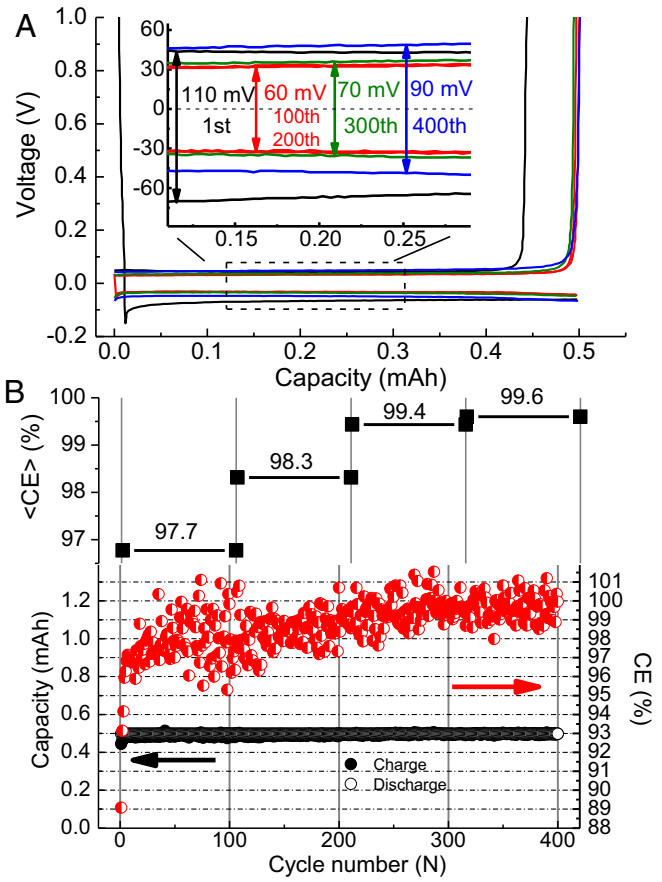


**Fig. 2.** Reversibility of LMA in HFF electrolytes (7 m LiFSI in FEC). The current density is 0.25 mA/cm$^2$ with the capacity of 0.5 mAh. (*A*) Li deposition–stripping profiles on Cu foil. (*B*) CE at cycle 1–400.

98.02% at the higher current densities (1 and 2 mA) (*SI Appendix*, Fig. S3). Symmetric Li/Li cell in *SI Appendix*, Fig. S4 also shows very stable and nearly constant polarization even after 300 h of charge–discharge without any short-circuiting. The cation ($Li^+$) and anion ($FSI^-$) transference numbers $t_\pm$ at 25 °C are determined by NMR spectroscopy (*SI Appendix*, Fig. S5 and Table S6). $t_+$ increases from 0.43 to 0.53 when the concentration increases from 1 to 7 m. From Sand's equation (42, 43), higher $t_+$ (lower $t_-$) of HFF delays anion depletion, which is beneficial for suppressing mode III morphological instabilities of LMA (1).

X-ray photoelectron spectroscopy (XPS) in Fig. 3 *A*–*C* reveals that the surface chemical components of cycled Li anode are mainly LiF, organic C–O group, $Li_2CO_3$, and $Li_2O$, derived from two possible ways: by the surface passivation film on the lithium anode ($Li_2O$, $Li_2CO_3$) due to sample transfer, and by the decomposition of electrolyte (LiF, organic C–O group, $Li_2CO_3$, and $Li_2O$). Before Ar ion sputtering, LiF, organic C–O group, residual LiFSI, and $Li_2CO_3$ were detected without $Li_2O$ signal. Sputtering depth profiling of the absolute intensity of SEI components (LiF, $Li_2O$, and $Li_2CO_3$) (Fig. 3 *B* and *C*) shows that from outer layer to inner layer, the components are LiF/$Li_2CO_3$, $Li_2CO_3$, and $Li_2O$. The strongest intensity of LiF and $Li_2CO_3$ occurs at an earlier stage after 2-min sputtering, but the intensity of $Li_2O$ continues to increase with the sputtering time. We thus conclude that all of LiF and a small part of $Li_2CO_3$ and $Li_2O$ are likely to originate from SEI formation by the decomposition of electrolyte, while most of $Li_2O$ and $Li_2CO_3$ probably belong to the inherent passivation film on Li metal. Surface chemistry analysis of cycled LMA further confirmed that the SEI layer contained a large amount of LiF. HF formation and attack of electrodes is a common concern in LIBs. FEC is known to be a HF generator with certain electrode materials like Si. However, in our case, considering that only LiF shows up without C–F signal, and also the fact that Ni or Mn dissolution and transfer are not detected at all from the LNMO cathode to the anode (*SI Appendix*, Fig. S6), we believe HF is completely absent in our system due to the HF scavenging effect of Li metal. Based on ours and others' experiments (44, 45), the following FEC reduction reaction, FEC + $Li^+ + e^- \rightarrow$ poly(VC) + LiF + $Li_2CO_3$, is proposed.

While LiF layer can shut down electron tunneling and stop SEI growth, it will take some time for it to form a completely covering layer on the surface. Electrochemical impedance spectra of LMA in HFF are shown in *SI Appendix*, Fig. S7. Fig. 3 *D* and *E* and *SI Appendix*, Fig. S8 show the deposited LMA morphologies in different electrolytes for identical current density (0.25 mA/cm$^2$) and deposition time. PC-based electrolytes clearly give more porous LMA, and the porosity decreases with increasing DFC. If we compare Fig. 3 *D* and *E* with Fig. 3 *F* and *G*, we see the long slender whiskers (diameter ~1 μm and aspect ratio >10) in PC are conspicuously missing in the high-DFC samples. These whiskers are determined to be mode II rather than mode III (1) because the Sand's time are very long for such low current density. Also, true dendrites which are long-range transport-limited tend to have branches. Different from PC, the growth of Li in LiFSI-FEC exhibits no long-aspect-ratio whiskers but much bigger and uniform grain size. Especially in HFF electrolyte (7 m LiFSI in FEC), the particle size exceeds 20 μm. As indicated by previous in situ transmission electron microscopy (TEM) observations (1), the growth of mode II Li whiskers usually starts by tensile stress-driven mechanical failure of SEI, followed by compressive stress-driven extrusion of lithium like toothpaste or volcanic eruption from a fumarole. At the potential of concern, SEI forms everywhere a conductive surface and electrolyte meet. In order for lithium deposition to continue, $Li^+$ in the electrolyte must diffuse through the SEI to meet with electron beneath the SEI, which causes compressive stress to build up in the lithium metal, and tensile stress to build up in the SEI layer on top. If the SEI layer is brittle and cannot plastically stretch, then inevitably it will fracture mechanically at some point (Fig. 3*H*) (1, 46), after which the lithium whisker can be squeezed out from the fumarole to relax the compressive stress via creep deformation. The same stress–relaxation causes Sn whisker formation in microelectronic solders. This will greatly increase the surface area. Also, the slender whisker geometry, as shown in the in situ TEM observations (1), is highly irreversible, since upon Li stripping it tends to narrow and neck first at the root due to younger/thinner SEI and lower impedance at root, causing loss of electrical connection to the rest of the whisker ("dead lithium"), and/or simply mechanically break off at the stem to become "lithium flotsam" (1). For these reasons, the suppression of whisker formation due to ductility of SEI formed in HFF electrolyte could be key for the high reversibility of LMA. It is already known that alkali halides including LiF are ductile in tension at room temperature and nonaqueous condition (34). Compared with $Li_2CO_3$, LiF has higher surface energy, which makes brittle fracture more difficult according to the Griffith fracture criterion. Meanwhile, LiF has a very small lattice constant among halides, and therefore Burgers vector, which allows easy plastic deformation. Thus, LiF generated by the decomposition of HFF electrolyte is good at suppressing morphological instabilities. Equiaxed Li particles without a preferential growth direction (Fig. 3*G*) are a positive trait against porosity growth (47, 48).

Cathode-side issues include compatibility with LNMO, oxidative stability of electrolyte, as well as corrosion of Al current collector. Highly concentrated electrolytes are typically beneficial with respect to the oxidation of solvent and Al corrosion

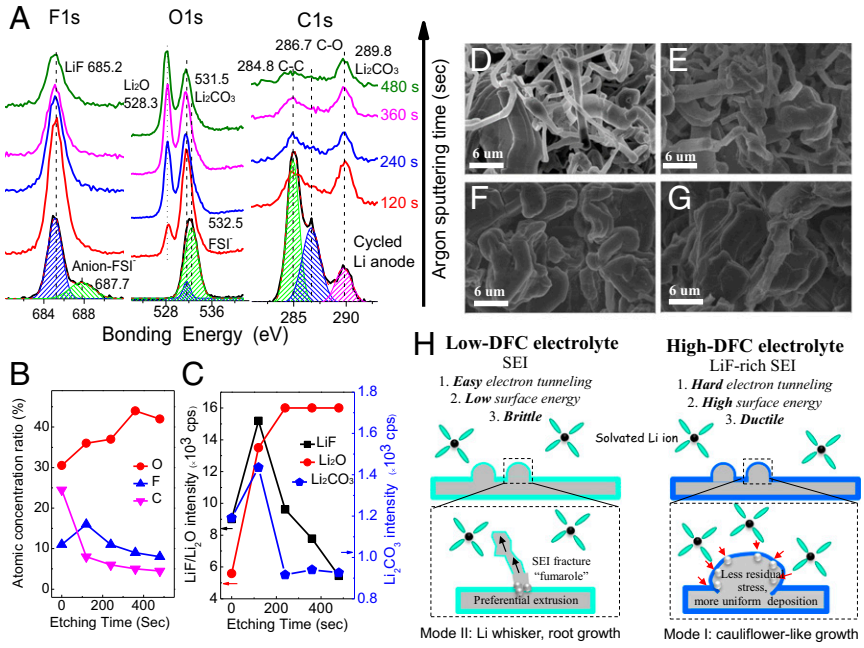


**Fig. 3.** Surface chemical analysis of cycled LMA (10 cycles at 0.5 mA, 1 h) in FF electrolyte (*A*–*C*). (*A*) XPS spectra of C, F, and O before and after Ar ion sputtering. Depth profiles with atomic concentration ratio (*B*) and with the intensity of SEI components (LiF, $Li_2O$, and $Li_2CO_3$) (*C*). Morphologies of Li deposition on Cu foil in different electrolytes [1 m LiTFSI in PC (*D*), 1 m LiFSI in PC (*E*), 1 m LiFSI in FEC (*F*), and 7 m LiFSI in FEC (*G*)]. The Li deposition current density is 0.5 mA/cm$^2$ and the deposited capacity is 1 mAh/cm$^2$. (*H*) Schematic diagram of corresponding Li growth mechanism in different electrolytes.

(17, 18, 22). Linear sweep voltammetry (LSV) with Al mesh as the working electrode (Fig. 4*A*) shows that high salt concentration is very effective in expanding the electrochemical stability window and suppressing Al corrosion. The onset of oxidation in HFF electrolyte was pushed to well above 5 V and no peak corresponding to Al corrosion occurs in the range of 3.5~5.5 V. The oxidation of electrolyte prefers to take place on oxygen with electron lone pairs, like the O=S bond in anion FSI and C=O bond in FEC. High concentration creates extensive Li cation coordination, resulting in enhanced stability of the electron lone pair of anion and solvent (18). In HFF, the minimal distance between solvent molecules and Al current collector should be increased due to high salt concentration and solvent surrounded by salt rather than the traditional solvation shell structure, resulting in lower electron tunneling current to the solvent. In addition, LiF formation on the cathode electrode confirmed by $F_{1s}$ and $Li_{1s}$ XPS spectra (*SI Appendix*, Fig. S9), which has a large bandgap (13.6 eV) and therefore a fast tunneling decay rate, is also favorable for Al anticorrosion and electrolyte stabilization (Fig. 4*B*) (19). Fig. 4*A* (*Inset*) displays their first charge–discharge profiles on active LiNMO electrode. For 1 m FF electrolyte, abnormal charge–discharge plateau, excessive charge capacity, and huge irreversible capacity loss signify oxidative decomposition of electrolyte before the delithiation of $LiNi_{0.5}Mn_{1.5}O_4$. But, in HFF (7 m), the batteries presented the high first discharge capacity of 123.8 mAh/g (LNMO) with CE of 92.78% and the superior cycle stability with the capacity retention of 94.26% after 150 cycles. Such capacities are comparable with the commercial carbonate-based electrolyte (SE: 1.0 M $LiPF_6$ in EC/DEC/DMC = 1:1:1 by weight, purchased from BASF) (Fig. 4*C* and *SI Appendix*, Fig. S10) with superabundant lithium. The charge–discharge polarization of the former does not obviously enlarge compared with the latter thanks to the higher $t_+$ in HFF, offsetting the relatively lower ionic conductivity of HFF electrolyte (1.25 mS/cm at 25 °C) (*SI Appendix*, Fig. S11) than commercial carbonate-based electrolyte (8~9 mS/cm at 25 °C). For comparison, identically concentrated carbonate electrolyte (7 m LiFSI in 1 L DMC) is also evaluated (*SI Appendix*, Fig. S12*B*), but is found to lead to serious Al corrosion once the potential is above 4.7 V, consistent with previous report (17). If the concentration is increased

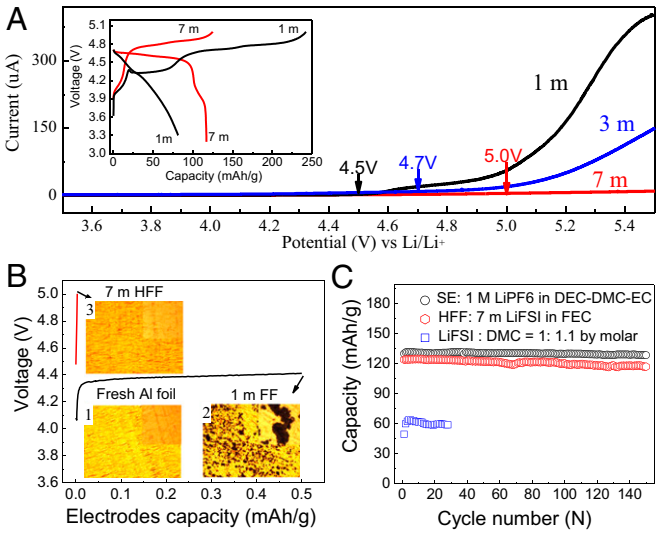


**Fig. 4.** Oxidation of HFF liquid electrolyte and its compatibility with the $LiNi_{0.5}Mn_{1.5}O_4$ cathode. (*A*) Concentration-dependent oxidation potential by LSV in three-electrode device (work electrode: Al mesh, counter- and reference electrodes: Li foil, scanning rate: 10 mV/s). (*Inset*) First charge–discharge profile of $LiNi_{0.5}Mn_{1.5}O_4$ in 1 m FF and 7 m HFF. (*B*) Al corrosion in 1 m FF and 7 m HFF at the constant current (0.5 mA) charge to 5 V. Optical microscopy images (OMIs) of (*B*, *1*) fresh Al foil, (*B*, *2*) OMIs of Al foil in 1 m FF electrolyte after charging 1 h at 0.5 mA, and (*B*, *3*) OMIs of Al foil in 7 m HFF after charging into 5 V at 0.2 mA. (*C*) Cycle life and CE of $LiNi_{0.5}Mn_{1.5}O_4$/HFF full cell with only 1.4× excess lithium. For reference, half-cell results using standard "SE" electrolyte (SE: 1.0 M $LiPF_6$ in EC/DEC/DMC = 1:1:1 by weight ratio) and highly concentrated DMC electrolyte (LiFSI: DMC = 1:1.1 by molar ratio) are also displayed, with ~100× excess lithium. The constant current of 0.5 mA is applied in all cells, corresponding to the rate of 0.36 C based on the theoretical capacity of $LiNi_{0.5}Mn_{1.5}O_4$ cathode (148 mAh/g).

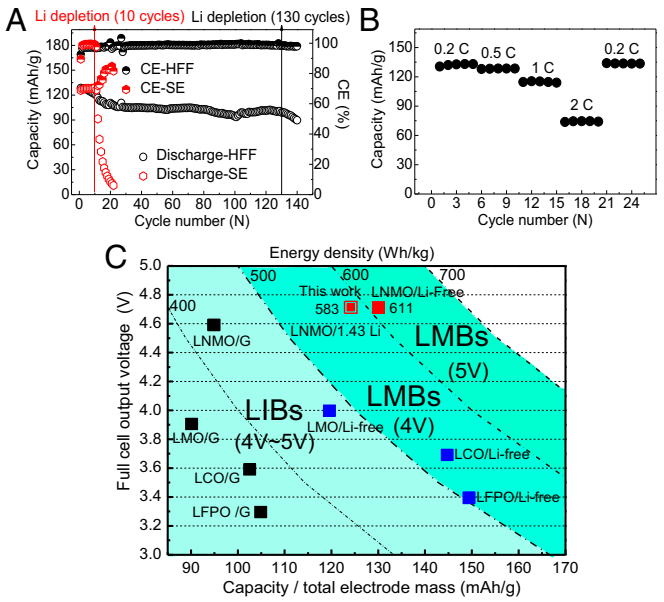


**Fig. 5.** Performance of $LiNi_{0.5}Mn_{1.5}O_4$/HFF or SE/Li system in full cell, where the Li mole ratio of cathode to anode is set up to 1 (1.43 mAh): 1.40 (2 mAh) in full cell. The initial Li anode (2 mAh) is prepared by depositing Li on Cu foil at a constant current of 0.05 mA for 40 h. (*A*) Cycle life and CE. The constant current of 0.5 mA is applied in full cell, corresponding to the rate of 0.36 C based on the theoretical capacity of cathode and the current density of 0.44 mA/cm$^2$ based on the current collect area of Cu foil. (*B*) Rate capability of full cell with HFF electrolyte. (*C*) Estimated output voltage, the real specific capacities of cathodes (*SI Appendix*, Table S1), and gravimetric energy densities based on the total electrode mass (cathode + anode) of different electrochemical couples. Black solid square: rechargeable graphite-based commercial LIBs; red and blue solid squares: rechargeable lithium metal-free batteries in which red and blue designate 5- and 4-V batteries, respectively. Except for the hollow red squares which represent the real energy density our 5-V lithium metal batteries, all of the other energy densities are calculated based on the theoretical capacity of electrodes.

further to 11 m (LiFSI:DMC = 1:1.1 by molar ratio), the battery shows very low capacity (<50 mAh/g) and much larger polarization due to the kinetic limitation of LiFSI-DMC (Fig. 4*C* and *SI Appendix*, Figs. S10 and S12*A*).

To demonstrate that the LMA with excellent CE actually leads to more competitive RLMB, we constructed full-cell battery with high mass loading LNMO (14.7 mg/cm$^2$, 1.83 mAh/cm$^2$, diameter 10 mm) as the cathode. Since LNMO already comes with a full portion of cyclable Li (the "baseline" portion), a truly ideal RLMB battery should use just bare Cu current collector (defined as "0× excess" or "Li-free battery") at the beginning. We have constructed and tested such a 0× excess RLMB: because Li have certain solubility in Cu and cyclable Li must also be consumed in SEI formation, the capacity fading of this 5-V Li-free battery is fast in the initial cycling with the capacity retention of 50.8% after 50 cycles (*SI Appendix*, Fig. S13). To demonstrate reasonable cycling, we predeposited some Li on the anode side ("0.5× excess," "1× excess," etc.), but not too much. From the Introduction we see that more than "3× excess" (e.g., 3 × 1.83 mAh/cm$^2$ worth of Li metal to start with) LMA would mean the RLMB is no longer competitive against LIB. In half-cell tests, Li metal chips (26 mg, 100 mAh, "~$10^2$× excess") were used as the anode (Fig. 4*C*), which is far from industrial-use scenarios. We have decided to demonstrate the efficacy of our electrolyte by using no more than "1.5× excess", which is a very stringent test for long-term cycling, which if successful, would mean the RLMB can be truly competitive against LIB. In such a parsimonious excess situation (Fig. 5*A* and *SI Appendix*, Fig. S14), a small difference in CE could lead to a huge disparity in cycle life. Assuming the cathode is 100% reversible without any capacity fade, the capacity of full cell will fade to zero after 100 cycles if 1% of the original cyclable Li inventory is lost per cycle (CE = 99%) on the LMA. The CE advantage of our FF electrolytes reflects in the limited excess Li anode we can use for long cycling. With commercial carbonate-based electrolytes, the same mass Li anode (2 mAh, 1.77 mAh/cm$^2$, diameter 12 mm) by Li deposition on Cu foil sustains less than 10 cycles due to low CE (<80%) (*SI Appendix*, Fig. S15), but maintains more than 130 cycles in HFF electrolyte. After 130 cycles, our anode exhausts its own 1.4× excess and begins to dip into the original baseline cyclable Li brought by the LNMO, and the full-cell capacity fades faster. The electrochemical performance of full cell at the different rates (0.2 C~0.5 C~1 C~2 C) is shown in Fig. 5*B* and *SI Appendix*, Fig. S16. The highest current density based on cathode electrode is above 3.66 mA/cm$^2$ at the rate of 2 C, at which point the capacity is still above 70 mAh/g (LNMO). Thus, our 5-V full cell has demonstrated a very good rate capability.

This result demonstrates the unique advantages of our proposed HFF electrolyte in 5-V Li metal full cell which not only has a good compatibility with cathode and wide enough stability window >5 V but also the capability to make the LMA more reversible. HFF is a liquid electrolyte satisfying simultaneously the requirements of a 5-V electrochemical window and >99% Li CE (Table 1). With its utilization, our proposed 5-V lithium metal battery presents much longer cycle life above 130 cycles with the capacity retention of 78% and ensuring an energy density of nearly 600 Wh/kg based on the total electrode masses (Fig. 5*C*) which is 30+% higher than graphite-based LNMO batteries and 50+% higher than the 4-V commercial graphite-based LIBs (*SI Appendix*, Tables S3–S6), with parsimonious excess Li (the mole ratio of LNMO/Li equal to 1:1.4) anode and high mass loading LNMO (14.7 mg/cm$^2$) cathode that are close to the industrial requirement. So far, increasing DFC has led to one formulation (LiFSI-FEC), demonstrating the feasibility of 5-V-class lithium metal battery. But, other fluorine-containing salts and fluoride solvents could be explored. This could also extend to high-DFC gel polymer electrolyte or the mixture ionic liquid-FF–based electrolytes for improving the full-cell performance, pushing RLMBs into the realm of practical applications.

## Experiment

The electrolytes are prepared by mol-salt in liter-solvent, which were coded by abbreviated concentrations (1 m, 2 m, 7 m, etc.). The 5-V Spinel

**Table 1. Comparison of electrolytes on 5-V RLMBs**

| Electrolyte components | Stable window, V | Al anticorrosion | Li CE, % | Fitness-for-service |
|---|---|---|---|---|
| SE: 1 M $LiPF_6$ in DEC-DMC-EC | 5 | Yes | <80 | No |
| EHC: 4 M LiFSI in DME | <4.5* | — | >99 | No |
| LFF: 1 m LiFSI in FEC | <4.5 | No | >98 | No |
| HFD: 7 m LiFSI in DMC | 5 | No | >98 | No |
| HFF: 7 m LiFSI in FEC | 5 | Yes | >99 | Yes |

*Electrochemical stability of ether-based and carbonate-based highly concentrated electrolyte (EHC and HFD) are evaluated in LiNMO/Li cell (*SI Appendix*, Figs. S12*B* and S17) which suffers from very serious overcharge and Al corrosion above 4.7 V, respectively.

$LiNi_{0.5}Mn_{1.5}O_4$ electrodes used in this experiment were produced at the US Department of Energy's (DOE) CAMP (Cell Analysis, Modeling, and Prototyping) Facility, Argonne National Laboratory. Composite electrodes were fabricated by compressing active materials, conductive additive, and binder at weight ratio of 84:8:8 on Al foil (20 μm). The total mass loading of the coating was 14.7 mg/cm$^2$, and the theoretical areal capacity was 1.83 mAh/cm$^2$. The cell was assembled in a CR2032-type coin cell with glass fiber separator. More details of the materials, characterizations, and electrochemical measurements are provided in *SI Appendix*.

**ACKNOWLEDGMENTS.** We thank Dr. Matthew Devany, director of the NMR facility of the Hunter College Chemistry Department. We acknowledge support by NSF ECCS-1610806. L.S. acknowledges support from One Hundred Talents Program of the Chinese Academy of Sciences. The electrodes were produced at the US DOE CAMP Facility, Argonne National Laboratory. The CAMP Facility is fully supported by the DOE Vehicle Technologies Program within the core funding of the Applied Battery Research for Transportation Program. Support for infrastructure/NMR Facility came from a grant from the National Institute on Minority Health and Health Disparities (8 G12 MD007599) awarded to Hunter College by the NIH.

1. Kushima A, et al. (2017) Liquid cell transmission electron microscopy observation of lithium metal growth and dissolution: Root growth, dead lithium and lithium flotsams. *Nano Energy* 32:271–279.
2. Lin D, Liu Y, Cui Y (2017) Reviving the lithium metal anode for high-energy batteries. *Nat Nanotechnol* 12:194–206.
3. Tikekar MD, Choudhury S, Tu ZY, Archer LA (2016) Design principles for electrolytes and interfaces for stable lithium-metal batteries. *Nat Energy* 1:16114.
4. Zhang S, Zhao K, Zhu T, Li J (2017) Electrochemomechanical degradation of high-capacity battery electrode materials. *Prog Mater Sci* 89:479–521.
5. Xu K (2014) Electrolytes and interphases in Li-ion batteries and beyond. *Chem Rev* 114:11503–11618.
6. Mogi R, et al. (2002) Effects of some organic additives on lithium deposition in propylene carbonate. *J Electrochem Soc* 149:A1578–A1583.
7. Ding F, et al. (2013) Effects of carbonate solvents and lithium salts on morphology and coulombic efficiency of lithium electrode. *J Electrochem Soc* 160:A1894–A1901.
8. Aurbach D, et al. (1995) The study of electrolyte-solutions based on ethylene and diethyl carbonates for rechargable Li batteries.1. Li metal anodes. *J Electrochem Soc* 142:2873–2882.
9. Aurbach D, Markovsky B, Shechter A, EinEli Y, Cohen H (1996) A comparative study of synthetic graphite and Li electrodes in electrolyte solutions based on ethylene carbonate dimethyl carbonate mixtures. *J Electrochem Soc* 143:3809–3820.
10. Aurbach D, Gofer Y, Benzion M, Aped P (1992) The behavior of lithium electrodes in propylene and ethylene carbonate–The major factors that influence Li cycling efficiency. *J Electroanal Chem* 339:451–471.
11. Aurbach D (2000) Review of selected electrode-solution interactions which determine the performance of Li and Li ion batteries. *J Power Sources* 89:206–218.
12. Fang Z, et al. (2017) Novel concentrated Li[$(FSO_2)$(n-$C_4F_9SO_2$)N]-based ether electrolyte for superior stability of metallic lithium anode. *ACS Appl Mater Interfaces* 9:4282–4289.
13. Zheng JM, et al. (2016) Highly stable operation of lithium metal batteries enabled by the formation of a transient high-concentration electrolyte layer. *Adv Energy Mater* 6:1502151.
14. Yamada Y, et al. (2015) Corrosion prevention mechanism of aluminum metal in superconcentrated electrolytes. *ChemElectroChem* 2:1687–1694.
15. Jeong SK, et al. (2008) Suppression of dendritic lithium formation by using concentrated electrolyte solutions. *Electrochem Commun* 10:635–638.
16. Fujii K, Wakamatsu H, Todorov Y, Yoshimoto N, Morita M (2016) Structural and electrochemical properties of Li ion solvation complexes in the salt-concentrated electrolytes using an aprotic donor solvent, N,N-Dimethylformamide. *J Phys Chem C* 120:17196–17204.
17. Wang J, et al. (2016) Superconcentrated electrolytes for a high-voltage lithium-ion battery. *Nat Commun* 7:12032.
18. McOwen DW, et al. (2014) Concentrated electrolytes: Decrypting electrolyte properties and reassessing Al corrosion mechanisms. *Energy Environ Sci* 7:416–426.
19. Matsumoto K, et al. (2013) Suppression of aluminum corrosion by using high concentration LiTFSI electrolyte. *J Power Sources* 231:234–238.
20. Qian JF, et al. (2016) Anode-free rechargeable lithium metal batteries. *Adv Funct Mater* 26:7094–7102.
21. Qian J, et al. (2015) High rate and stable cycling of lithium metal anode. *Nat Commun* 6:6362.
22. Yoshida K, et al. (2011) Oxidative-stability enhancement and charge transport mechanism in glyme-lithium salt equimolar complexes. *J Am Chem Soc* 133:13121–13129.
23. Suo L, Hu YS, Li H, Armand M, Chen L (2013) A new class of solvent-in-salt electrolyte for high-energy rechargeable metallic lithium batteries. *Nat Commun* 4:1481.
24. Gao Y, et al. (2017) Interfacial chemistry regulation via a skin-grafting strategy enables high-performance lithium-metal batteries. *J Am Chem Soc* 139:15288–15291.
25. Zhang ZC, et al. (2013) Fluorinated electrolytes for 5 V lithium-ion battery chemistry. *Energy Environ Sci* 6:1806–1810.
26. Jung HG, Hassoun J, Park JB, Sun YK, Scrosati B (2012) An improved high-performance lithium-air battery. *Nat Chem* 4:579–585.
27. Shiraishi S, Kanamura K, Takehara Z (1999) Surface condition changes in lithium metal deposited in nonaqueous electrolyte containing HF by dissolution-deposition cycles. *J Electrochem Soc* 146:1633–1639.
28. Lu Y, Tu Z, Archer LA (2014) Stable lithium electrodeposition in liquid and nanoporous solid electrolytes. *Nat Mater* 13:961–969.
29. Choudhury S, Archer LA (2016) Lithium fluoride additives for stable cycling of lithium batteries at high current densities. *Adv Electron Mater* 2:1500246.
30. Zhang XQ, Cheng XB, Chen X, Yan C, Zhang Q (2017) Fluoroethylene carbonate additives to render uniform Li deposits in lithium metal batteries. *Adv Funct Mater* 27:1605989.
31. Zheng J, et al. (2017) Electrolyte additive enabled fast charging and stable cycling lithium metal batteries. *Nat Energy* 2:17012.
32. Richards WD, Miara LJ, Wang Y, Kim JC, Ceder G (2016) Interface stability in solid-state batteries. *Chem Mater* 28:266–273.
33. Ozhabes Y, Gunceler D, Arias TA (2015) Stability and surface diffusion at lithium-electrolyte interphases with connections to dendrite suppression. arXiv:1504.05799.
34. Scott WD, Pask JA (1963) Deformation and fracture of polycrystalline lithium fluoride. *J Am Ceram Soc* 46:284–293.
35. Parker ER (1961) Status of ductile ceramic research (ASTM International, West Conshohocken, PA), ASTM STP283.
36. Schroder K, et al. (2015) The effect of fluoroethylene carbonate as an additive on the solid electrolyte interphase on silicon lithium-ion electrodes. *Chem Mater* 27:5531–5542.
37. Markevich E, et al. (2014) Fluoroethylene carbonate as an important component in electrolyte solutions for high-voltage lithium batteries: Role of surface chemistry on the cathode. *Langmuir* 30:7414–7424.
38. Younesi R, Veith GM, Johansson P, Edstrom K, Vegge T (2015) Lithium salts for advanced lithium batteries: Li-metal, Li-$O_2$, and Li-S. *Energy Environ Sci* 8:1905–1922.
39. Jin Y, et al. (2017) Self-healing SEI enables full-cell cycling of a silicon-majority anode with a coulombic efficiency exceeding 99.9%. *Energy Environ Sci* 10:580–592.
40. Gu WT, et al. (2016) Lithium-iron fluoride battery with in situ surface protection. *Adv Funct Mater* 26:1507–1516.
41. Shkrob IA, Marin TW, Zhu Y, Abraham DP (2014) Why bis(fluorosulfonyl)imide is a "magic anion" for electrochemistry. *J Phys Chem C* 118:19661–19671.
42. Chazalviel J (1990) Electrochemical aspects of the generation of ramified metallic electrodeposits. *Phys Rev A* 42:7355–7367.
43. Sand HJS (1901) On the concentration at the electrodes in a solution, with special reference to the liberation of hydrogen by electrolysis of a mixture of copper sulphate and sulphuric acid. *Philos Mag* 1:45–79.
44. Michan AL, et al. (2016) Fluoroethylene carbonate and vinylene carbonate reduction: Understanding lithium-ion battery electrolyte additives and solid electrolyte interphase formation. *Chem Mater* 28:8149–8159.
45. Okuno Y, Ushirogata K, Sodeyama K, Tateyama Y (2016) Decomposition of the fluoroethylene carbonate additive and the glue effect of lithium fluoride products for the solid electrolyte interphase: An ab initio study. *Phys Chem Chem Phys* 18:8643–8653.
46. Park MS, et al. (2014) A highly reversible lithium metal anode. *Sci Rep* 4:3815.
47. Mehdi BL, et al. (2016) The impact of Li grain size on coulombic efficiency in Li batteries. *Sci Rep* 6:34267.
48. Aurbach D, Zinigrad E, Cohen Y, Teller H (2002) A short review of failure mechanisms of lithium metal and lithiated graphite anodes in liquid electrolyte solutions. *Solid State Ion* 148:405–416.

Supporting information

# Fluorine-donating electrolytes enable highly reversible 5 V Li metal batteries

Liumin Suo[1,2], Weijiang Xue[2], Mallory Gobet[3], Steve G. Greenbaum[3], Chao Wang[2], Yuming Chen[2], Wan-Lu Yang[4], Yang-Xing Li[4*] and Ju Li[2*]

[1] Key Laboratory for Renewable Energy, Beijing Key Laboratory for New Energy Materials and Devices, Beijing National Laboratory for Condensed Matter Physics, Institute of Physics, Chinese Academy of Sciences, School of Physical Sciences, University of Chinese Academy of Sciences, Beijing 100190, China

[2] Department of Nuclear Science and Engineering and Department of Materials Science and Engineering, Massachusetts Institute of Technology, Cambridge, MA 02139, USA.

[3] Department of Physics and Astronomy, Hunter College of CUNY, 695 Park Avenue, New York, NY 10065, USA.

[4] Watt Laboratory, Central Research Institute, Huawei Technologies Co., LTD., Bantian, Longgang District, Shenzhen 518129, China.

**Materials.** Lithium bis(trifluoromethane sulfonyl) imide ($LiN(SO_2CF_3)_2$, LiTFSI) (>98%), LiFSI, $LiClO_4$ and FEC were purchased from Tokyo Chemical Industry, Oakwood Products, Inc. and Sigma-Aldrich and Alfa respectively. All solvents (FEC and PC) were purified by the 4Å molecular sieve before used. The electrolytes are prepared by mol-salt in liter-solvent), which were coded by abbreviated concentrations Lithium bis(trifluoromethane sulfonyl) imide ($LiN(SO_2CF_3)_2$, LiTFSI) (>98%), LiFSI, $LiClO_4$ and FEC were purchased from Tokyo Chemical Industry, Oakwood Products, Inc. and Sigma-Aldrich and Alfa respectively. All solvents (FEC and PC) were purified by the 4Å molecular sieve before used.

**Characterizations**. Scanning electron microscopy (SEM) image was taken by Zeiss Merlin High-resolution Scanning electron microscope operating at 5 kV. X-ray photoelectron spectroscopy (XPS, aka ESCA) analysis was performed on Kratos AXIS with high depth resolution (10 nm or less), good elemental sensitivity (0.1 to 0.01 atomic percent), and lateral resolution down to 10 μm. $Ar^+$ etching was conducted at an argon partial pressure of $<10^{-8}$ Torr. All the samples were recovered from 2032 coin cell configuration after electrochemical cycling. The samples were washed by DME three times and then dried under vacuum for two hours before XPS measurement. A portable transfer vessel was used to process samples in glove-box and loaded into the XPS without exposure to air. The NMR diffusion experiments were done with a 400 SB Bruker AVANCE III spectrometer (9.4 T). Self-diffusion coefficients of FEC and $FSI^-$ ($^{19}F$ NMR), and $Li^+$ ($^7Li$ NMR) were measured at 25°C using a stimulated echo sequence with bipolar pulses . Gradient strength was arrayed (16 values, linear increase,

$g$ = 0-45 G/cm) for each experiment. Gradient pulse duration was δ/2 = 1.1-4 ms and diffusion delay was Δ = 200-750 ms.

**Electrochemical Measurements**. The ionic conductivity was measured with electrochemical impedance spectroscopy (EIS) using Gamry Reference 3000 over a temperature range of 10 to 50 °C. The samples were equilibrated in a thermostated water-bath, and at each set temperature the sample was left standing for at least 1 h before EIS were collected. The conductivity cell constants were pre-determined using 0.01M aqueous KCl standard solution at 25 °C. Linear sweep voltammetry (LSV) was applied to determinate the electrochemical stability window at a scanning rate of 10 mV/s using Al mesh as working electrode and Li strip as the counter and the reference electrode, which was carried out using Gamry electrochemical work station. Al mesh were thoroughly cleaned ultrasonically in high purity alcohol, and then washed three times with high purity water and dried before measurement. The diameter of cathode electrode is 10 mm. The Li anode electrodes used in half and full cell are thick Li chip (MTI Corporation) and thin pre-deposited Li on Cu foil (ϕ = 12 mm), respectively. Pre-deposited Li anode was obtained at a constant current of 0.05 mA for 40 hours. The cell was assembled in CR2032-type coin cell using 5 V Spinel $LiNi_{0.5}Mn_{1.5}O_4$ cathode, Li metal anode and glass fiber as separator. The cells were cycled galvanostatically on a Land BT2000 battery test system at room temperature.

**The definition of Coulombic efficiency (CE)**. The CE values are defined with the following "clean-slate" procedure: one first pulls out all the $Li^+$ one can pull out in a copper-backed anode, making sure there is no cyclable Li reserve (although SEI, which contains non-cyclable Li, can exist physically) on the anode side. One then electrochemically deposit $Q_{re}$ fresh $Li^+$ to the anode with $U_{max} \rightarrow U_{min}$, in the form of metallic lithium with varying degree of porosity. Lastly, one pulls $Q_{ox}$ $Li^+$ out of the anode with $U_{min} \rightarrow U_{max}$, and compute $CE \equiv Q_{ox}/Q_{re}$.

**Electrochemical impedance spectra (EIS) of LMA in HFF electrolyte**. The data was collected in symmetric Li/Li cell in intervals of ten hours to characterize the growth of SEI. Fig. S7*B* shows that the charge-transfer resistance semi-circle increased from 50 Ω to 160 Ω with the resting time, indicated continuous SEI growth on lithium metal anode. The increase is asymptotic, so the growth rate of SEI was very fast in the initial stage and then gradually tapered off at the range of 150 ~160 Ω after 80 hours.

**The definition of Donatable Fluorine Concentration (DFC).** Donatable Fluorine Concentration (DFC) is defined straightforwardly as the molar sum of donatable F of salt and solvent molecules in 1-liter electrolyte solution. Considering that our electrolyte preparation by the ratio of salt to solvent with molar (salt) to liter (solvent) and the volume change before and after the mixture, we measured the densities of electrolytes listed in Table S5. Take 1 m LiFSI-FEC for example, the weight ratio of LiFSI to FEC is 187.07 to 1410 (density of FEC: 1.41 g/cc) which are correspond to the weight percentage of

11.7 % and 88.3 % respectively. Thus, 1.51 g/cc should have 0.9455 mmol LiFSI and 12.57 mmol FEC with F contribution number of 2 (LiFSI) and 1 (FEC). Finally, DFC of 1 m LiFSI-FEC is equal to 14.46 (0.9455*2 + 12.57).

**The measurement of Ion transference number in LiFSI-FEC system**. Ion transference number is the fraction of the total current carried in an electrolyte by a given ion. The cation transference number ($t^+$) and anion transference number ($t^-$), corresponding to the fraction of current carried out by the lithium ions and $FSI^-$ ions respectively, were calculated by using following equations.

$$t^+ = \frac{D_{\mathrm{Li}^+}}{D_{\mathrm{Li}^+} + D_{\mathrm{TFSI}^-}} \qquad (1)$$

$$t^- = \frac{D_{\mathrm{TFSI}^-}}{D_{\mathrm{Li}^+} + D_{\mathrm{TFSI}^-}} \qquad (2)$$

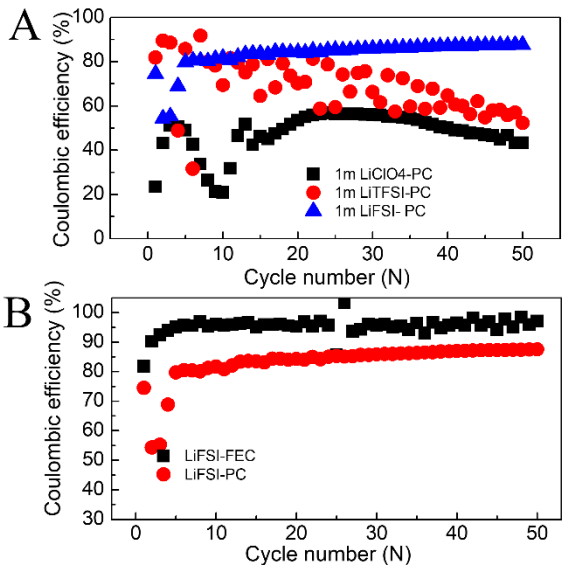


**Fig. S1.** The Coulombic efficiency of Li metal anode **(a)** in fluoride based salts (1m LiTFSI and LiFSI) and non-fluoride salt (1 m $LiClO_4$) dissolved in PC solvent, **(b)** in fluorinated (FEC) and non-fluorinated solvent (PC) contained 1 m LiFSI.

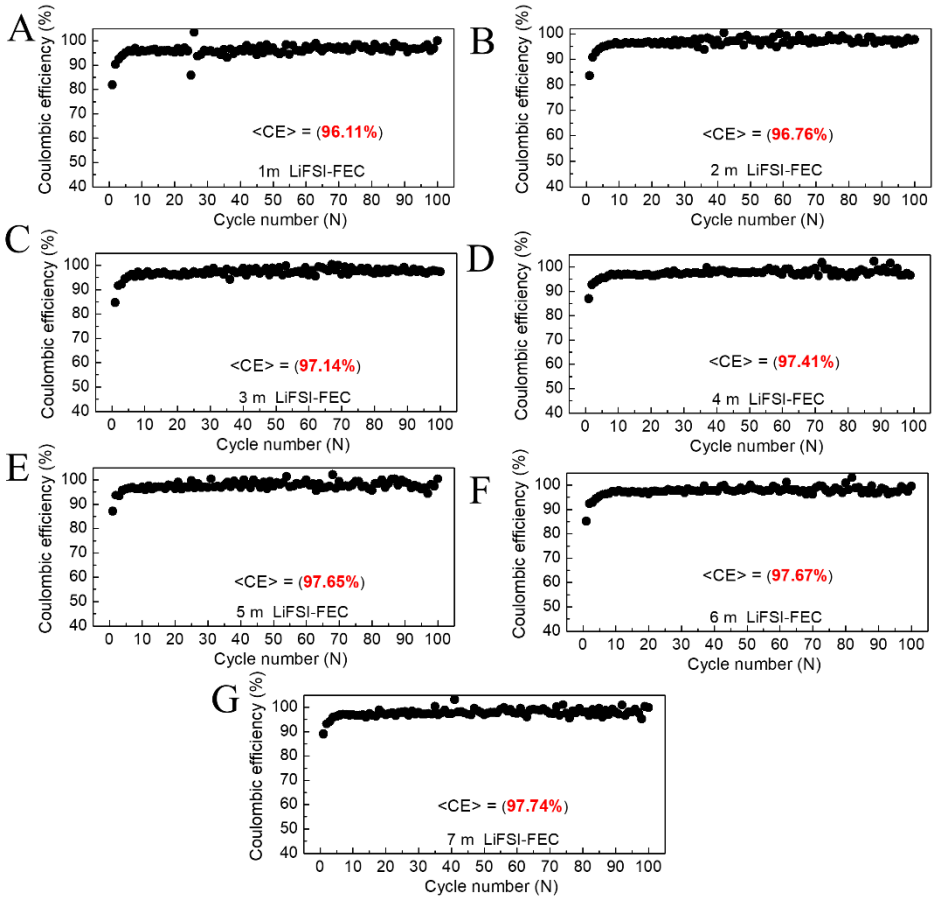


**Fig. S2**. Coulombic efficiencies (CE) of Li metal anode in different concentrated LiFSI in FEC and its average Coulombic efficiencies <CE> in the first 100 cycles, which is corresponding to Figure 1a and Figure 1c. (a) 1 m, (b) 2 m, (c) 3 m, (d) 4 m, (e) 5 m, (f) 6 m and (g) 7 m.

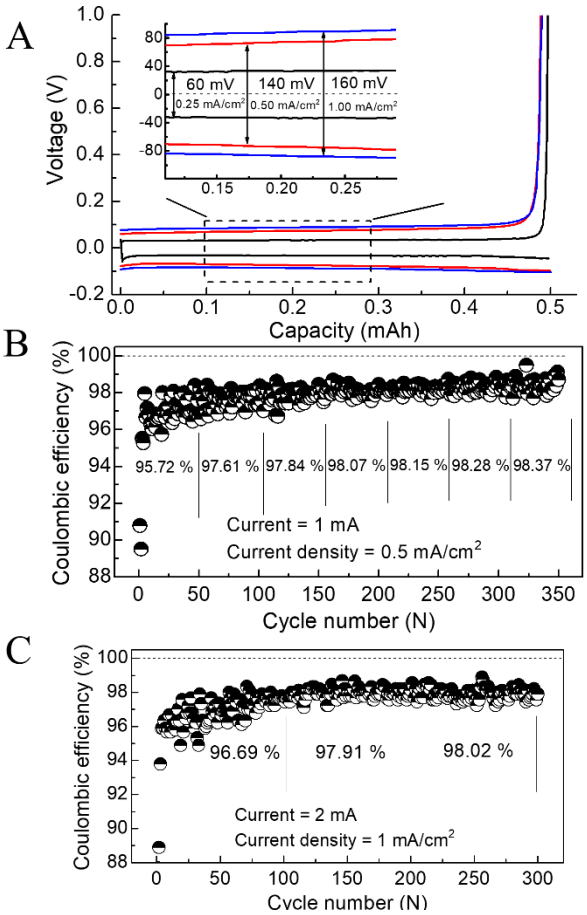


**Fig. S3**. The reversibility of Li metal anode in High Concentrated Full Fluoride-based (HFF) electrolytes (7 m LiFSI in FEC). (*A*) The initial Li deposition-dissolution profiles on Cu foil at different current density (0.25 mA/cm$^2$, 0.50 mA/cm$^2$ and 1.00 mA/cm$^2$), (*B*) and (*C*) the cycle Coulombic efficiencies of Li anode at 0.50 mA/cm$^2$ and 1.00 mA/cm$^2$.

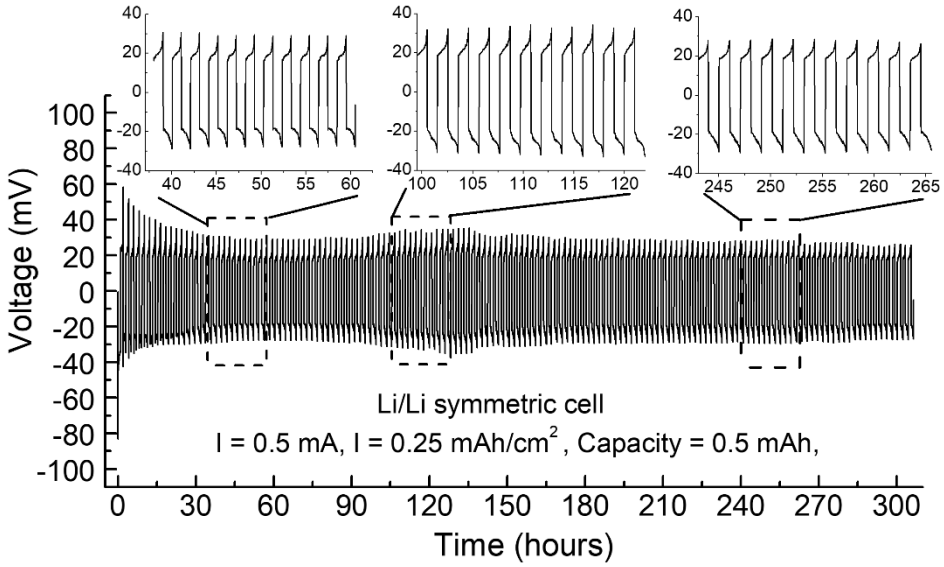


**Fig. S4**. The reversibility of Li metal anode in Symmetric Li/Li cell with HCFF electrolyte (7 m LiFSI in

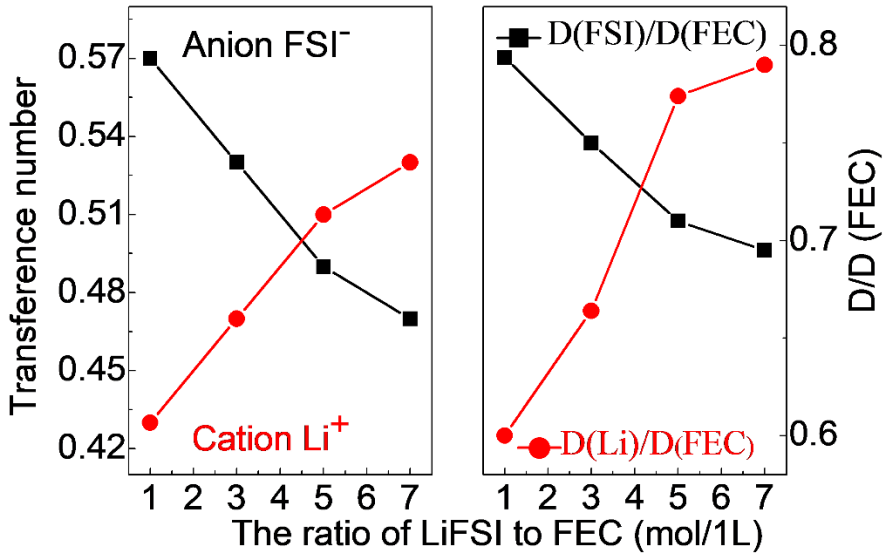


**Fig. S5. Full Fluoride-based (HFF) electrolytes (LiFSI-FEC).** Cation (Li ion) and anion ($FSI^-$) transference numbers and the self-diffusion coefficient ratio of $Li^+/FSI^-$ to FEC at 25 °C.

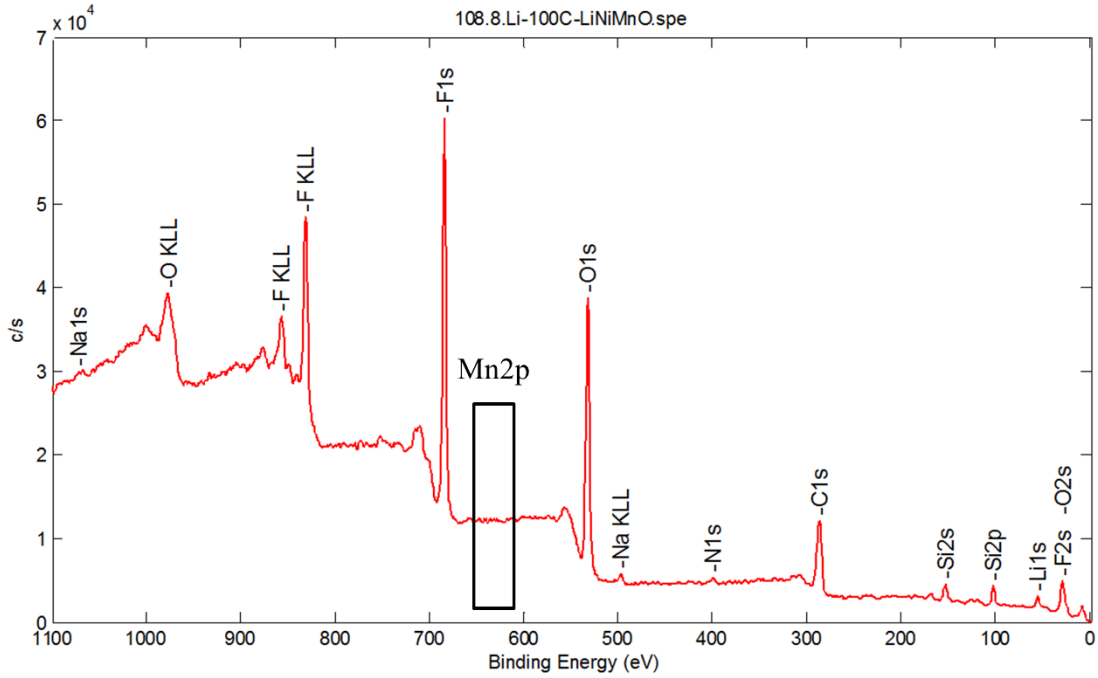


**Fig. S6**. XPS spectrum of Lithium anode after 100 cycles in half cell (LiNiMnO4/HFF/Li)

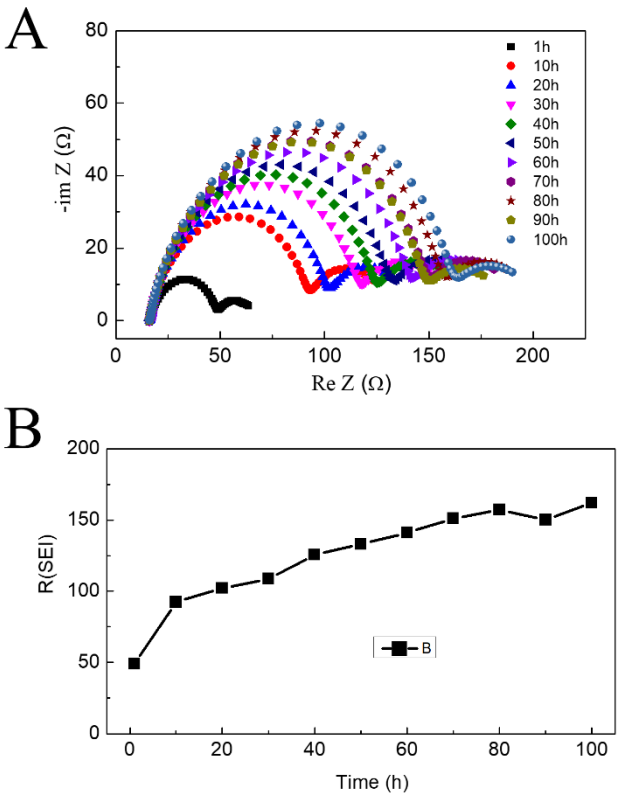


**Fig. S7.** The impedance of symmetric Li/Li cell with the resting time. (*A*) The impedance spectra of symmetric Li/Li cell in FF electrolyte at different rest times and (*B*) The change of SEI resistance with the increasing of resting time.

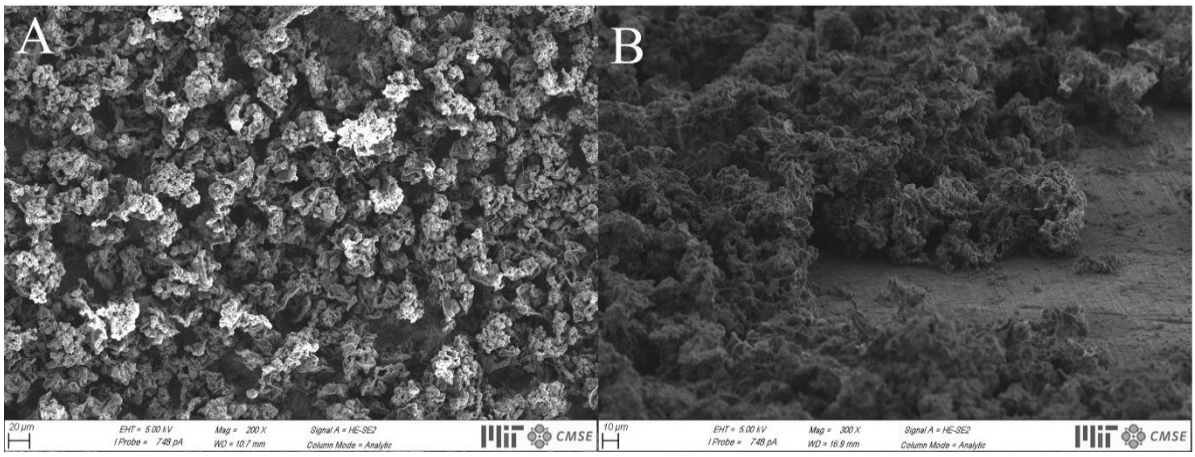


**Fig. S8.** The morphology of Li deposition on Cu foil. (*A*) Low magnification SEI image, (*B*) The cross-section view of SEM image.

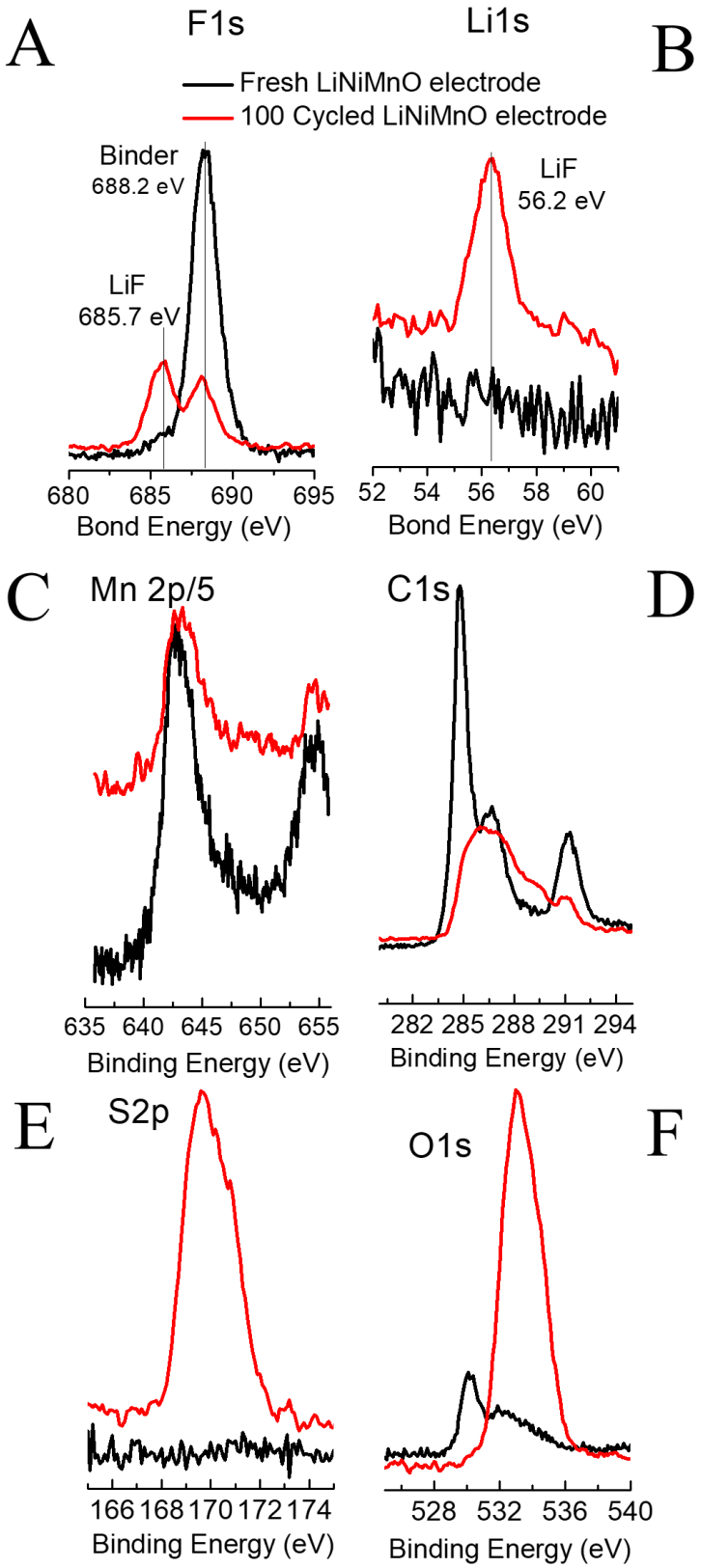


**Fig. S9.** XPS spectra of LiNMO electrode in HCFF electrolyte before and after 100 cycles. (*A*) $F_{1s}$ and (*B*) $Li_{1s}$, (*C*) Manganese element, Mn 2p/5, (*D*) Carbon element, C1s, (*E*) Sulfur element, S2p and (*F*) Oxygen element, O1

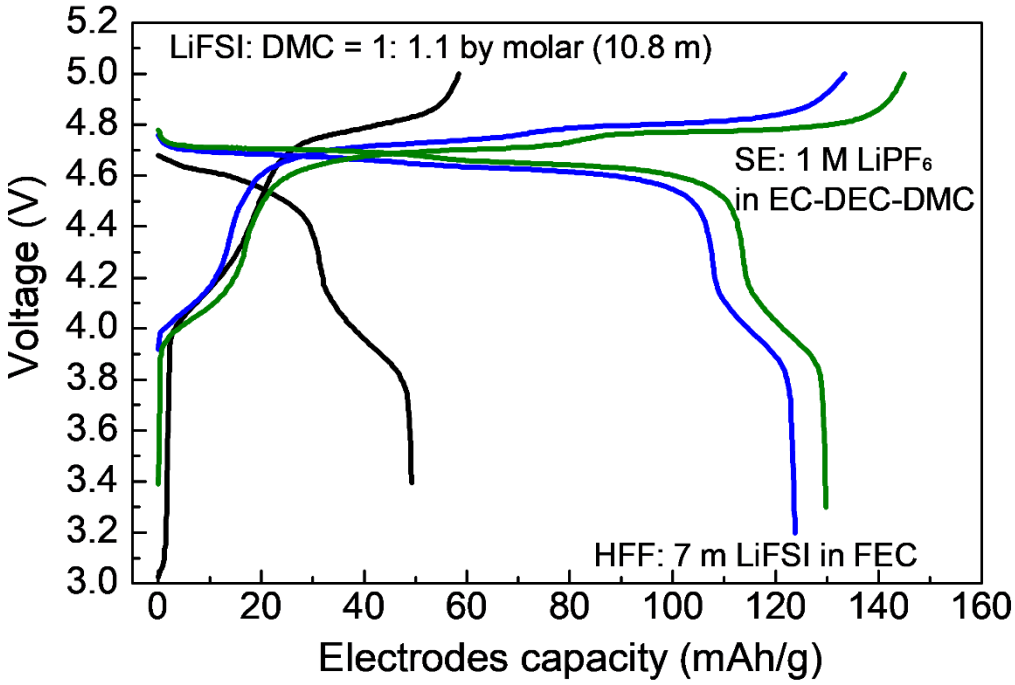


**Fig. S10.** The galvanostatic charge-discharge profiles of $LiNi_{0.5}Mn_{1.5}O_4$/HCFF electrolyte, LiFSI:DMC=1.1.1 by molar and SE/Li system in half cell, where the Li mole ratio of cathode to anode is above 1:100.

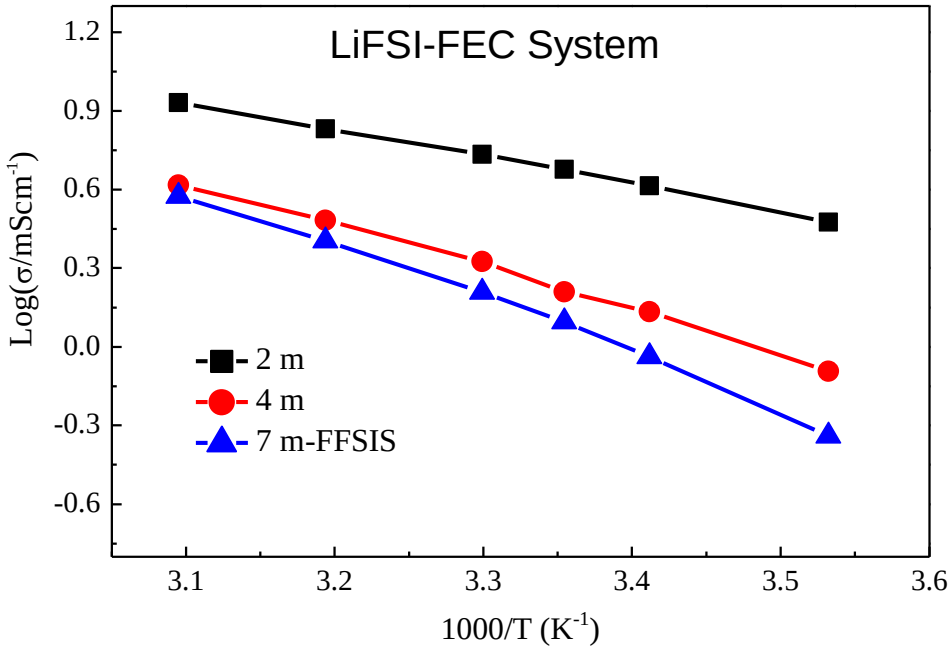


**Fig. S11.** Arrhenius plots of Lithium ion conductivity (σ) of LiFSI-FEC system in temperature range of 10 ºC ~ 50 ºC.

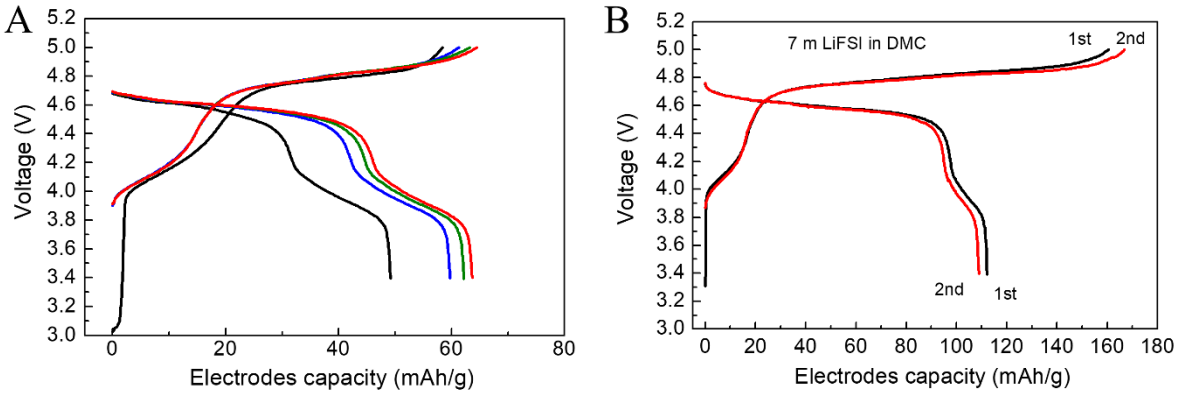


**Fig. S12.** The galvanostatic charge-discharge profiles of $LiNi_{0.5}Mn_{1.5}O_4$/ Li system in half cell, where the Li mole ratio of cathode to anode is above 1:100. (*A*) HFC：LiFSI : DMC = 1:1.1 by molar ratio, (*B*) 7 m LiFSI in DMC.

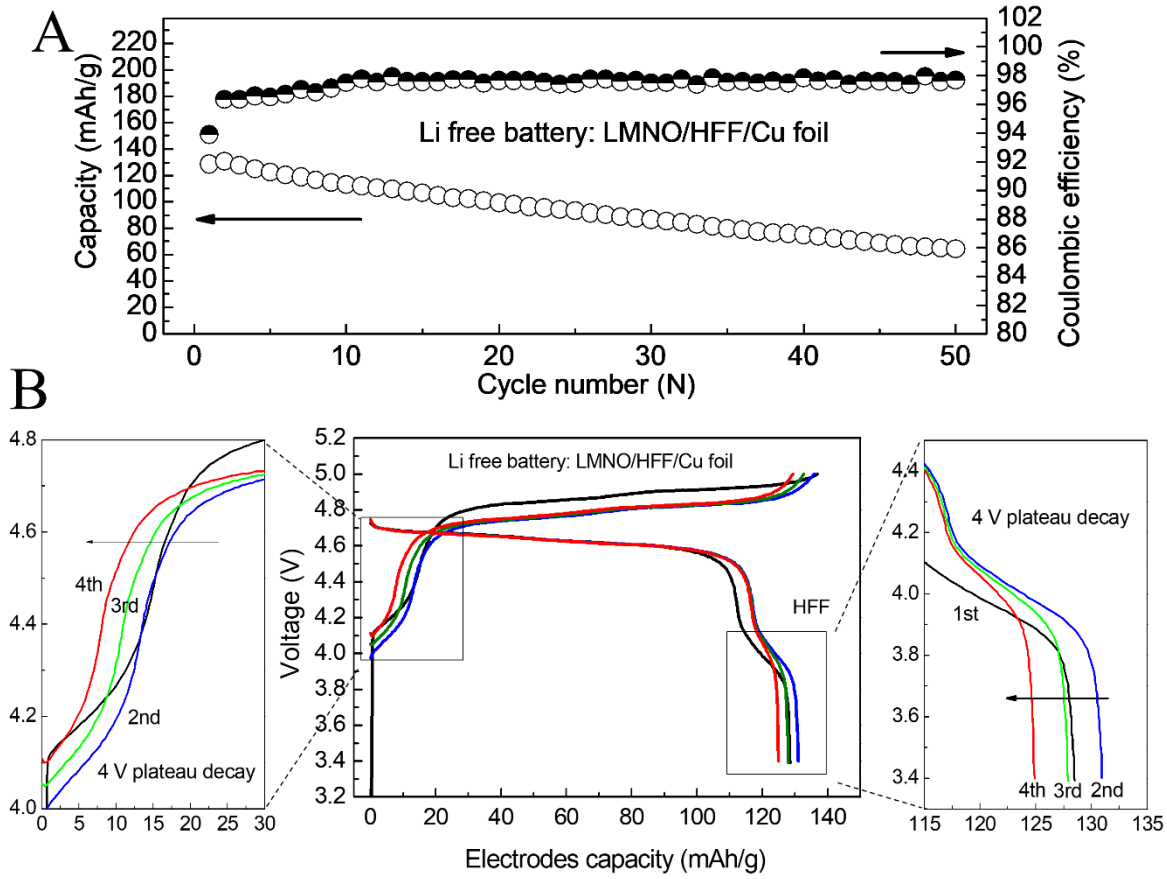


**Fig. S13.** The electrochemical performance of 5 V Li free battery constructed on LiNMO/HFF/Cu foil. (*A*) the cyclic life and columbic efficiency, (*B*) the charge-discharge initial profiles ($1^{st} \sim 4^{th}$).

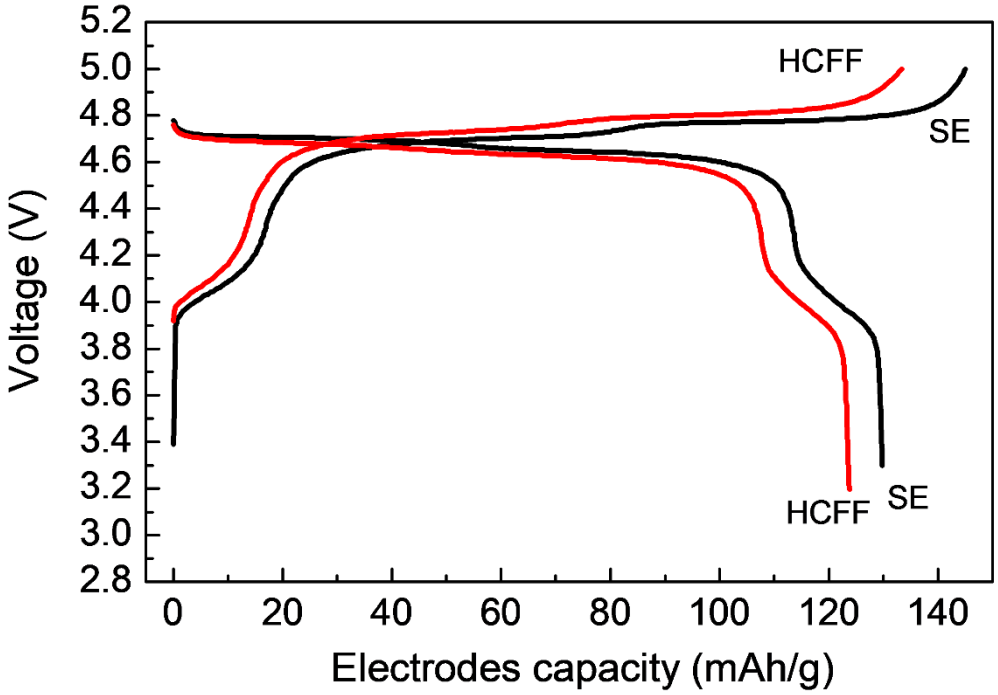


**Fig. S14.** Galvanostatic charge-discharge profiles of $LiNi_{0.5}Mn_{1.5}O_4$/HFF or SE /Li system in full cell

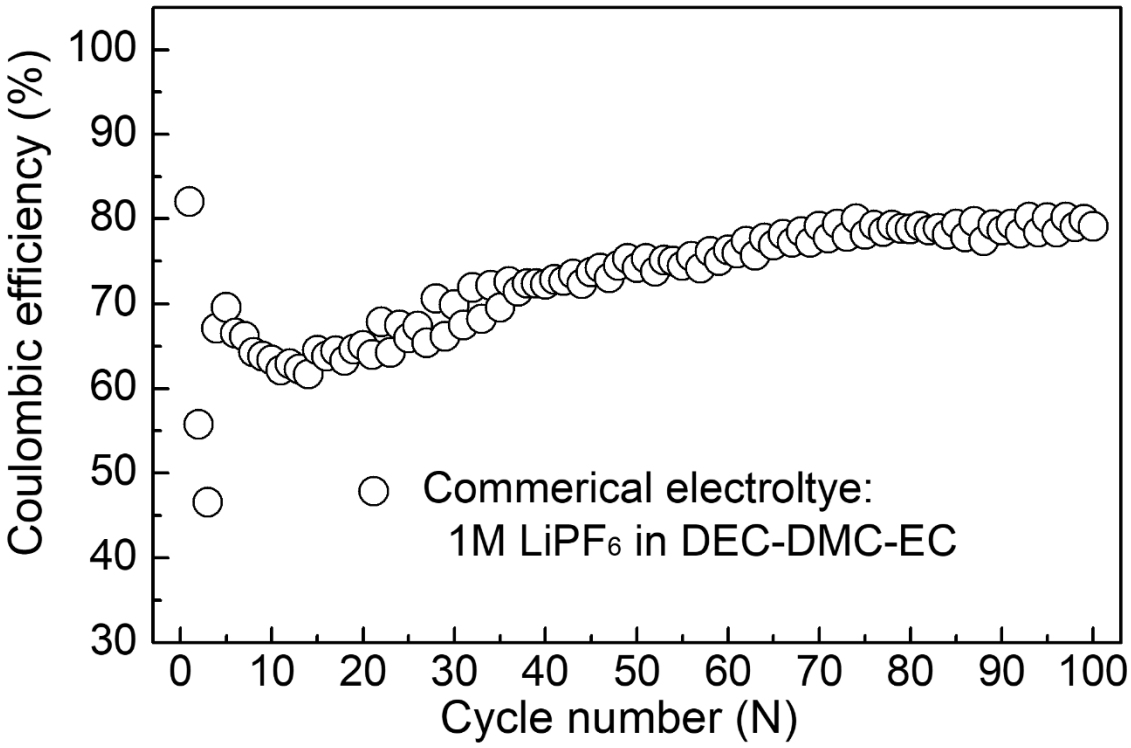


**Fig. S15.** The cycle coulombic efficiencies of Li anode in commercial electrolyte: 1M $LiPF_6$ in DEC-DMC-EC (BASF). The deposited/dissolved current density is 0.25 mA/cm$^2$ with the capacity of 0.5 mAh.

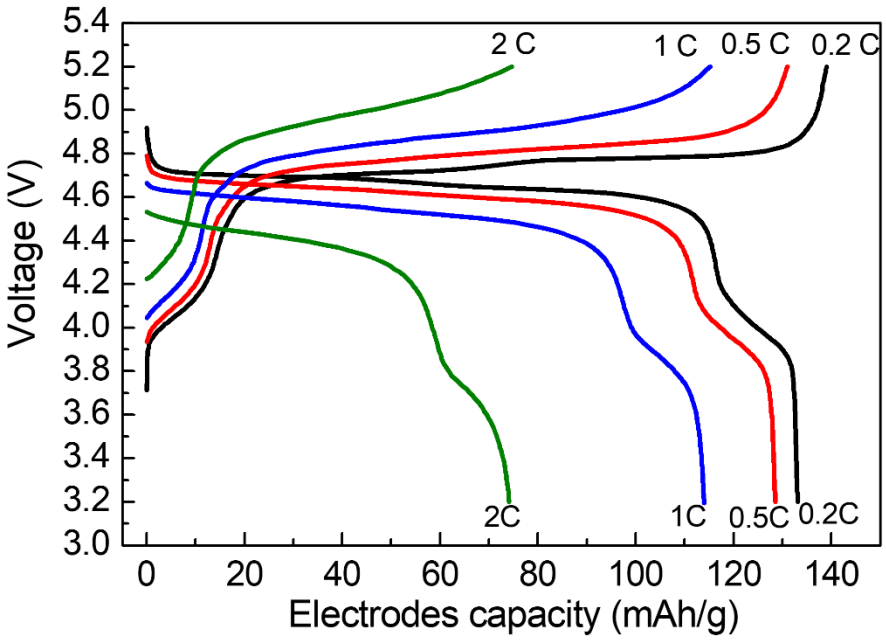


**Fig. S16.** The rate capability of full cell with HFF electrolyte. (*C*). The charge-discharge profile at different rates (0.2C, 0.5C, 1C and 2C), (*D*) the discharge capacity at the different rates.

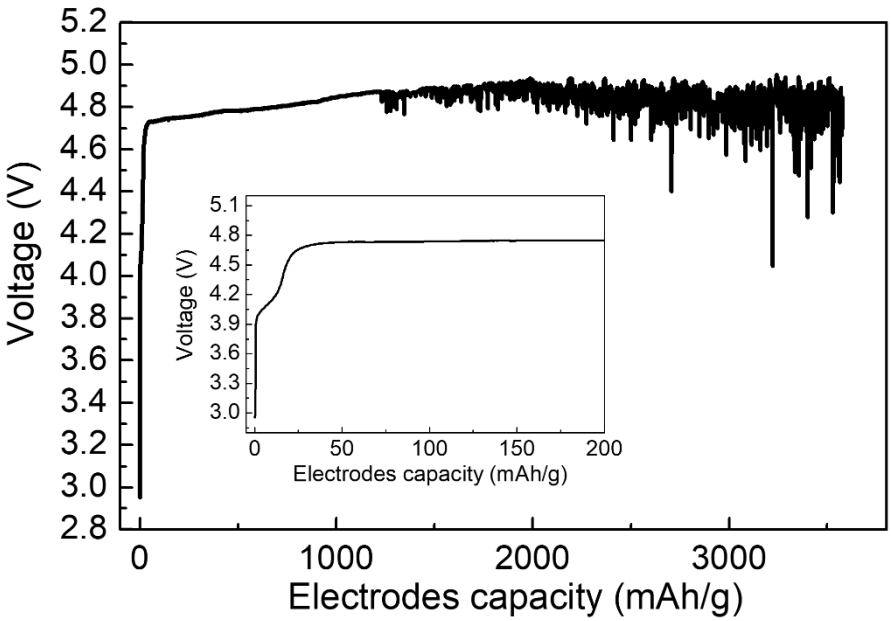


**Fig. S17.** The first charge profile of LiNMO/Li with 4M LiFSI in DME electrolyte

**Table S1.** The capacity and operating voltage of cathodes

| Cathode | Voltage vs Li (V) | Theoretical capacity (mAh/g) | The real capacity |
|---|---|---|---|
| $LiFePO_4$ | 3.4 | 170 | 150 |
| $LiCoO_2$ | 3.7 | 145 | 145 |
| LiMn2O4 | 4.0 | 148 | 120 |
| $LiNi_{0.5}Mn_{1.5}O_4$ | 4.7 | 146 | 130 |

**Table S2.** The capacity and operating voltage of graphite and Li metal anodes

| Anode | Voltage vs Li (V) | Theoretical capacity (mAh/g) | The real capacity (mAh/g) |
|---|---|---|---|
| Graphite | 0.1 | 375 | 360 |
| Li metal | 0 | 3860 | 3860 |

**Table S3.** The energy density calculation of graphite based Li ion batteries

| Graphite based Li ion batteries | Output Voltage (V) | Theoretical capacity (mAh/g) | The real capacity (mAh/g) | Energy density (Wh/kg) |
|---|---|---|---|---|
| $LiFePO_4$/G | 3.3 | 170/375 | 150 /360 | 349 |
| $LiCoO_2$/G | 3.6 | 145/375 | 145/360 | 373 |
| $LiMn_2O_4$/G | 3.9 | 148/375 | 120/360 | 351 |
| $LiNi_{0.5}Mn_{1.5}O_4$/G | 4.6 | 146/375 | 130/360 | 440 |

**Table S4.** The energy density calculation of Li-Free batteries

| Li-Free batteries | Output Voltage (V) | Theoretical capacity (mAh/g) | The real capacity (mAh/g) | Energy density (Wh/kg) |
|---|---|---|---|---|
| $LiFePO_4$ | 3.4 | 170 | 150 | 510 |
| $LiCoO_2$ | 3.7 | 145 | 145 | 536 |
| $LiMn_2O_4$ | 4.0 | 148 | 120 | 480 |
| $LiNi_{0.5}Mn_{1.5}O_4$ | 4.7 | 146 | 130 | 611 |

**Table S5.** DFC of different F donated electrolytes

| Electrolyte | Salt (mol) | Solvent (Liter) | Density (g/cc) | DFC |
|---|---|---|---|---|
| 1 m $LiClO_4$-PC | 1 mol | 1 L | 1.24 | 0 |
| 1 m LiTFSI-PC | 1 mol | 1 L | 1.27 | 0.851 |
| 1 m LiFSI-PC | 1 mol | 1 L | 1.26 | 1.810 |
| 1 m LiFSI-FEC | 1 mol | 1 L | 1.51 | 14.46 |
| 2 m LiFSI-FEC | 2 mol | 1 L | 1.56 | 15.12 |
| 3 m LiFSI-FEC | 3 mol | 1 L | 1.58 | 15.47 |
| 4 m LiFSI-FEC | 4 mol | 1 L | 1.60 | 15.79 |
| 5 m LiFSI-FEC | 5 mol | 1 L | 1.61 | 15.99 |
| 6 m LiFSI-FEC | 6 mol | 1 L | 1.66 | 16.58 |
| 7 m LiFSI-FEC | 7 mol | 1 L | 1.68 | 16.86 |

**Table S6.** NMR data for LiFSI-FEC electrolytes

| Electrolyte mol/ 1L | Self-diffusion coefficient (in $m^2/s$) at 25°C | | | Li ion Transference Number | Anion Transference Number |
|---|---|---|---|---|---|
| LiFSI-FEC | $D_{FEC}$ | $D_{FSI^-}$ | $D_{Li^+}$ | $t_{Li}$ | $t_{FSI}$ |
| 1m | 1.70E-10 | 1.35E-10 | 1.02E-10 | 0.43 | 0.57 |
| 3m | 5.48E-11 | 4.11E-11 | 3.64E-11 | 0.47 | 0.53 |
| 5m | 1.76E-11 | 1.25E-11 | 1.31E-11 | 0.51 | 0.49 |
| 7m | 9.56E-12 | 6.65E-12 | 7.53E-12 | 0.53 | 0.47 |